Molecular gas on large circumgalactic scales at $z = 3.47$

M. Ginolfi,[1,2,3]★ R. Maiolino,[2,3]★ T. Nagao,[4] S. Carniani,[2,3] F. Belfiore,[2,3] G. Cresci,[5]
B. Hatsukade,[6] F. Mannucci,[5] A. Marconi,[5,7] A. Pallottini,[2,3,8] R. Schneider[1]
and P. Santini[1]

[1]*INAF/Osservatorio Astronomico di Roma, Via di Frascati 33, I-00040 Monte Porzio Catone, Italy*
[2]*Cavendish Laboratory, University of Cambridge, 19 J.J Thomson Avenue, Cambridge CB3 0HE, UK*
[3]*Kavli Institute for Cosmology, University of Cambridge, Madingley Road, Cambridge CB3 0HA, UK*
[4]*Research Centre for Space and Cosmic Evolution, Ehime University, 790-8577 Ehime, Japan*
[5]*INAF/Osservatorio Astrofisico di Arcetri, Largo E. Fermi 5, I-20125, Firenze, Italy*
[6]*National Astronomical Observatory of Japan, 2-21-1 Osawa, Mitaka, 181-8588 Tokyo, Japan*
[7]*Dipartimento di Fisica e Astronomia, Universita' di Firenze, Via G. Sansone 1, I-50019, Sesto Fiorentino (Firenze), Italy*
[8]*Scuola Normale Superiore, Piazza dei Cavalieri 7, I-56126 Pisa, Italy*

ABSTRACT

We report the ALMA observations of the most massive (star-forming) galaxy in the redshift range $3 < z < 4$ within the whole Great Observatories Origins Deep Survey South field (GOODS-S) field. We detect a large elongated structure of molecular gas around the massive primeval galaxy, traced by the CO(4−3) emission, and extended over 40 kpc. We infer a mass of the large gaseous structure of $M_{gas} \sim 2$–$6 \times 10^{11}\,M_{\odot}$. About 60 per cent of this mass is not directly associated with either the central galaxy or its two lower mass satellites. The CO extended structure is also detected in continuum thermal emission. The kinematics of the molecular gas shows the presence of different components, which cannot be ascribed to simple rotation. Furthermore, on even larger scales, we detect nine additional CO systems within a radius of 250 kpc from the massive galaxy and mostly distributed in the same direction as the CO elongated structure found in the central 40 kpc. The stacked images of these CO systems show detections in the thermal continuum and in the X-rays, suggesting that these systems are forming stars at a rate of 30–120 $M_{\odot}\,yr^{-1}$. We suggest that the extended gas structure, combined with its kinematic properties, and the gas-rich star-forming systems detected on larger scales, are tracing the inner and densest regions of large-scale accreting streams, feeding the central massive galaxy. These results corroborate models of galaxy formation, in which accreting streams are clumpy and undergo some star formation (hence enriching the streams with metals) even before accreting onto the central galaxy.

Key words: ISM: molecules – galaxies: evolution – galaxies: general – galaxies: high-redshift – infrared: general.

1 INTRODUCTION

Modern theories of galaxy evolution and cosmological numerical simulations predict that massive galaxies, especially in the early stages of their formation, accrete a large amount of gas from the intergalactic medium (IGM), mostly through large-scale filamentary structures funnelling gas into the galaxy dark matter (DM) halo towards the disc (Dekel et al. 2009; Genel et al. 2012; Silk & Mamon 2012).

Such gas replenishment has to occur continuously throughout the cosmic time and more efficiently at early epochs, to sustain the intense star formation observed in primeval systems (Dekel et al. 2009; Kereš et al. 2009; Sánchez Almeida et al. 2014). These theoretical claims are observationally supported by the finding that high-redshift star-forming galaxies are characterized by gas depletion time-scales of the order of, or shorter than, 1 Gyr, hence requiring that fresh gas must be supplied at a high rate across a significant fraction of the galaxy lifetime, at least while populating the so-called main sequence (e.g. Tacconi et al. 2013; Genzel et al. 2015; Scoville et al. 2016). The need for prolonged star formation

★ E-mail: michele.ginolfi@oa-roma.inaf.it (MG); r.maiolino@mrao.cam.ac.uk (RM)

time-scales sustained by gas accretion is also inferred from studies of the chemical enrichment of spiral galaxies (e.g. Tinsley 1981; Matteucci & Francois 1989; Matteucci 2014).

The additional gas needed to support star formation can be provided by the IGM, feeding massive primeval galaxies via gas accretion through cosmic streams (Sancisi et al. 2008; Fraternali 2014). Theoretical models and numerical simulation have thoroughly investigated the role of gas accretion in galaxy evolution. The standard view of 'hot accretion mode' has persisted for years, arguing that galaxies form out of collapsing, virialized gas that forms an hot halo and then slowly cools, and settles in a disc (Rees & Ostriker 1977; White & Rees 1978; Fall & Efstathiou 1980). This view has been substantially modified in the past decade and the new paradigm of 'cold accretion mode' predicts that, at early cosmic epochs, the majority of gas enters the DM halo in the cold phase along filaments feeding the disc growth, without significant shock heating, at least at $z > 3.5$ (Birnboim & Dekel 2003; Dekel & Birnboim 2006; Ocvirk, Pichon & Teyssier 2008; Brooks et al. 2009; Kereš et al. 2009; Stewart et al. 2011). It should be noted that such models expect that cold streams are halted in massive galaxies ($M_\star > 10^{11}\,\mathrm{M_\odot}$) at $z < 3$–3.5 as a consequence of halo shock heating (Cattaneo et al. 2006; Dekel et al. 2009).

Our current understanding of cold gas inflows is largely based only on such models, as observational studies have been severely limited by the difficulty of tracing such cold gas accretion.

Attempts have been made in tracing the distribution of circumgalactic gas around high-redshift galaxies by looking at distinct kinematic signatures in absorption systems (along the line of sight of background quasars) produced by accreting material (e.g. Bouché et al. 2013; Prochaska, Lau & Hennawi 2014). Unfortunately, this approach is limited by the sparseness of aligned quasar-high-redshift galaxies pairs and by the fact that only one line of sight is usable, which results in degeneracies on the inferred circumgalactic medium (CGM) distribution. Another powerful tool to observe the extended gas reservoir surrounding high-redshift galaxies is through direct imaging of Lymanα (Lyα) emission due to recombination radiation following photoionization (sometimes referred to as 'fluorescence') powered by powerful ultraviolet (UV) sources (Lowenthal et al. 1990; Haardt & Madau 1996; Bunker, Marleau & Graham 1998; Cantalupo et al. 2005; Geach et al. 2009; Kollmeier et al. 2010). Successful ultra-deep observations of hyper-luminous quasars at $z > 2$ have indeed revealed giant Lyα haloes with projected linear sizes larger than 100 kpc (Cantalupo, Lilly & Haehnelt 2012; Cantalupo et al. 2014; Hennawi et al. 2015; Borisova et al. 2016). Recently, extensive integral field spectroscopic surveys have led to the first detection of the two-dimensional distribution of spatially extended Lyα emission also around low-mass ($\sim 10^8$–$10^9\,\mathrm{M_\odot}$) star-forming galaxies at $z > 3$ (Patrício et al. 2016; Wisotzki et al. 2016; Vanzella et al. 2017), revealing that Lyα haloes appear to be ubiquitous even among 'normal' galaxies at high redshift.

Although such results seem to confirm what predicted by models, revealing the extended gaseous structures expected to exist around primeval galaxies, the physical properties and the nature of the cosmic accreting gas expected by theories are still debated. Indeed, observations of Lyα haloes are only able to offer limited insight into the nature of the CGM because of (1) the possibility of tracing only the warm ionized phase of the gas surrounding primeval galaxies (which is generally a small fraction of total), (2) the degeneracies affecting the physical parameters estimated from radiative transfer modelling of Lyα emission and (3) the inability to infer detailed information about the kinematics of the three-dimensional spatially

extended gas, because of both Lyα absorption and the resonant nature of the line.

Such limits allow observations to only partly confirm models, leaving the observational evidence of gas cosmic streams feeding high-redshift galaxies still sparse and debated. However, due to the increasing accuracy of numerical cosmological simulations, the theoretical scenario has substantially evolved over the last few years. While initial theories were predicting inflows of nearly pristine gas (Birnboim & Dekel 2003; Kereš et al. 2005; Dekel & Birnboim 2006), recent simulations have shown that cooling and gravitational collapse may happen in gas streams, possibly leading to star formation within them, resulting in metal enrichment prior to delivery onto the massive galaxy (Pallottini, Gallerani & Ferrara 2014; Ceverino et al. 2016; Nelson et al. 2016; Pallottini et al. 2017). More specifically, Dekel et al. (2009) claim that about 30 per cent of the inflowing gas is converted into stars along the filamentary streams, before reaching the central massive galaxy. In support of this scenario, Bouché et al. (2013, 2016) report, through absorption spectroscopy at high-z, the detection of inflowing gas significantly enriched in metals ($Z \sim 0.4\,Z_\odot$). This scenario opens up new possibilities for the cosmic gas accretion to be investigated, within dense environment, by exploiting some of the classical tracers of star formation and molecular gas.

In this study, we report the Atacama Large Millimeter/submillimeter Array (ALMA) observations of an extended molecular gas structure around a massive star-forming galaxy at $z = 3.47$ located in an overdense region (see Section 2), which may provide new insights about gas accretion onto primeval galaxies.

Throughout the paper, we assume a ΛCDM cosmology with $\Omega_\mathrm{m} = 0.3$, $\Omega_\Lambda = 0.7$ and $h = 70\,\mathrm{km\,s^{-1}}$. 1 arcsec at $z \sim 3.5$ corresponds to ~ 7.47 kpc.

2 CANDELS-5001: A MASSIVE GALAXY IN AN OVERDENSE REGION AT $z = 3.47$

Candels-5001 (ID 4417 in the GOODS-MUSIC catalogue; Grazian et al. 2006) is a Lyman-break-selected star-forming galaxy at redshift $z = 3.47$ (measured through the [O III]5007 Å transition; Maiolino et al. 2008).

Candels-5001 is the most massive galaxy ($M_\star \sim 1.9 \times 10^{10}\,\mathrm{M_\odot}$; Santini et al. 2015) in the redshift range $3 < z < 4$ within the whole 150 arcmin^2 covered by the Great Observatories Origins Deep Survey South field (GOODS-S). It is actively forming stars at a rate of $\sim$200–250 $\mathrm{M_\odot\,yr^{-1}}$ (Troncoso et al. 2014). This galaxy is also detected in the X-rays; however, Fiore et al. (2012) exclude the presence of an active galactic nucleus (AGN) and show that the X-ray emission is fully consistent with what expected from the observed star formation rate. Table 1 summarizes the main properties of the galaxy.

Two star-forming lower mass companions are located at a distance of about 7–15 kpc (i.e. $\sim$1–2 arcsec) from Candels-5001 and are likely in the process of merging (as suggested by their kinematics; see Section 4.2).

Candels-5001 is located in a large-scale overdensity of galaxies traced by a clear, prominent spike in the distribution of spectroscopic redshifts over GOODS-S[1] (Fig. 1), suggesting that it is the massive central galaxy in a forming protocluster. This has been recently confirmed by the analysis of Franck & McGaugh (2016), based on

---

[1] We collected all available spectroscopic redshifts for galaxies around $z \sim 3$–4 in GOODS-S from the GOODS Multiwavelength Southern Infrared Catalog (GOODS-MUSIC; Santini et al. 2009).

RA J2000	DEC J2000	Redshift	$12+\log(O/H)^a$	$\log(M_{star}/M_\odot)^b$	$F(CO_{4-3})^c$ Jy km s^{-1}	$\log(M_{H_2}/M_\odot)^c$	$F_{cont.}(103\,GHz)$ μJy	$\log(SFR)^d$ M$_\odot$ yr^{-1}
03:32:23:336	$-27.51.56.862$	3.473	$8.41^{+0.10}_{-0.10}$	$10.27^{+0.38}_{-0.11}$	0.13 ± 0.02	$11.09^{+0.17}_{-0.25}$	36.1 ± 9.6	2.33 ± 0.31

^{a}Obtained using the empirical calibration derived by Curti et al. (2017).

^{b} Santini et al. (2015).

^{c}This work.

^{d}From the extinction-corrected Hβ emission (Troncoso et al. 2014).
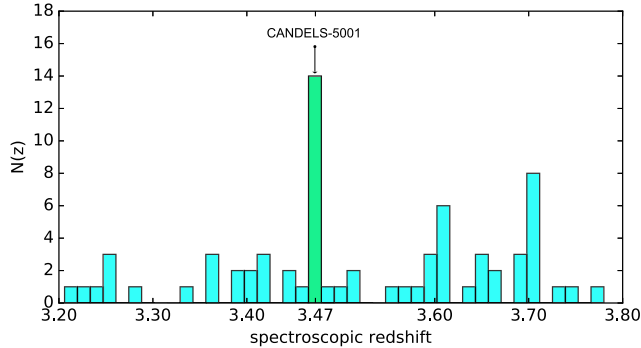
Figure 1. Distribution of spectroscopic redshifts of the galaxies optically identified in the GOODS-S field. The arrow indicates the redshift of Candels-5001.

an accurate galaxy overdensity (δ_{gal}) selection criterion applied on a catalogue of spectroscopically identified candidate protoclusters.

In such an overdense region, metal and dust enrichment in the IGM is supposed to be efficiently enhanced by galactic winds and outflows.

This peculiar environment, combined with the achieved ALMA sensitivity and angular resolution ($\sim$60 arcsec), makes the selected target the right candidate to investigate cosmic gas accretion at high redshift by observing the molecular gas phase.

3 ALMA OBSERVATIONS AND DATA REDUCTION

Observations were carried out during ALMA cycle 1, in 2013 November, making use of 30 antennas (12 m diameter), with a maximum baseline of 1.2 km, but most of the antennas were distributed in a relatively compact configuration. This results into a synthesized beam full-width at half-maximum (FWHM) of about 1.5 arcsec in size, if using the natural weighting of the visibilities, but maps with a resolution of 1 arcsec can be achieved by using different (Briggs, with robustness parameter of 2) weighting of the baselines (as discussed later on). The antennas were pointed at the optical position of Candels-5001. A total bandwidth of 7.5 GHz was employed in Band 3, using four wavebands between 90 and 106 GHz. The primary beam FWHM at such frequencies is $\sim$60 arcsec. One of the wavebands was centred at 103.1 GHz, which is the frequency of the CO J = 4−3 transition at the target redshift, i.e. $z = 3.473$. The other sidebands were used for continuum measurements. A total of 116 min of on-source integration time, distributed over three execution blocks ($\sim$40 min each), were obtained.

The ALMA observatory staff performed initial data calibration, as part of standard data processing and delivery. The calibrated visibility data have been then re-analysed, performing additional flagging of bad channels, using CASA version 4.5.3 (McMullin et al. 2007). The data have been imaged initially using the CASA natural weighting of the visibility data to create continuum map
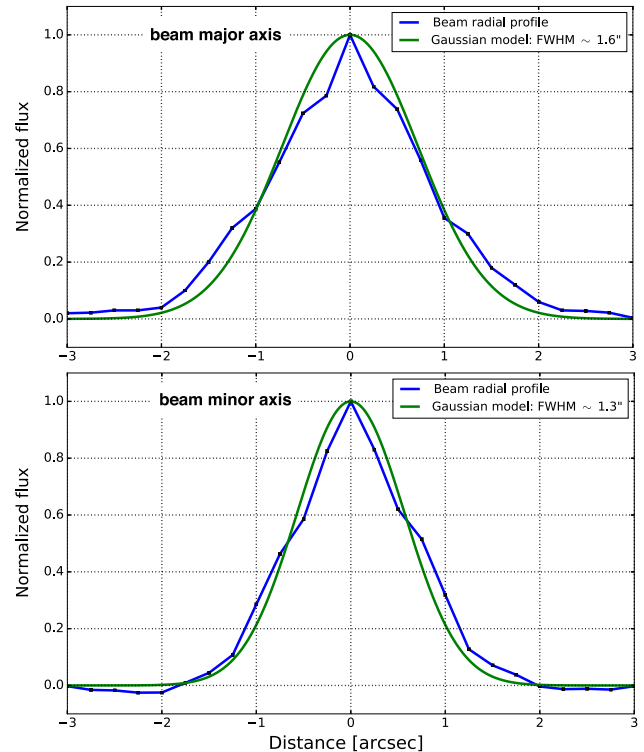

Figure 2. Upper (lower) panel: the beam radial profile along its major (minor) axis and a Gaussian profile are shown. In both cases, there is a deviation from Gaussianity on small distances, allowing for some sensitivity on scales smaller than the beam FWHM.

and data cubes. We achieve an rms sensitivity of 9.6 μJy beam^{-1} for the continuum image and 6 mJy beam^{-1} km s^{-1} in the waveband centred on the CO J = 4−3 transition, where the latter rms is given in spectral bins of 20 km s^{-1} ($\sim$7 MHz). The sensitivity in the other three sidebands is lower since the noise is, on average, 10 per cent higher. The absolute flux systematic uncertainty (associated with the flux calibration) is $\sim$10 per cent.

A slight astrometric alignment of less than 0.5 arcsec in the NW direction has been performed to match the ALMA data with the optical images (see Appendix A for a discussion). This level of systemic offsets between optical and ALMA data has been found in other cases (e.g. Maiolino et al. 2015; Dunlop et al. 2017) and are likely associated with either the astrometric accuracy of the ALMA phase calibrator and/or the astrometric accuracy of the optical images. However, we emphasize that the key results are not affected by the slight astrometric adjustment.

We note that the small relative number of antennas on long distances in our configuration results in a poorly covered visibilities plane on long baselines and, in turn, in a synthesized beam that is not Gaussian, as illustrated in Fig. 2. These long baselines provide some sensitivities on scales smaller than the beam FWHM.
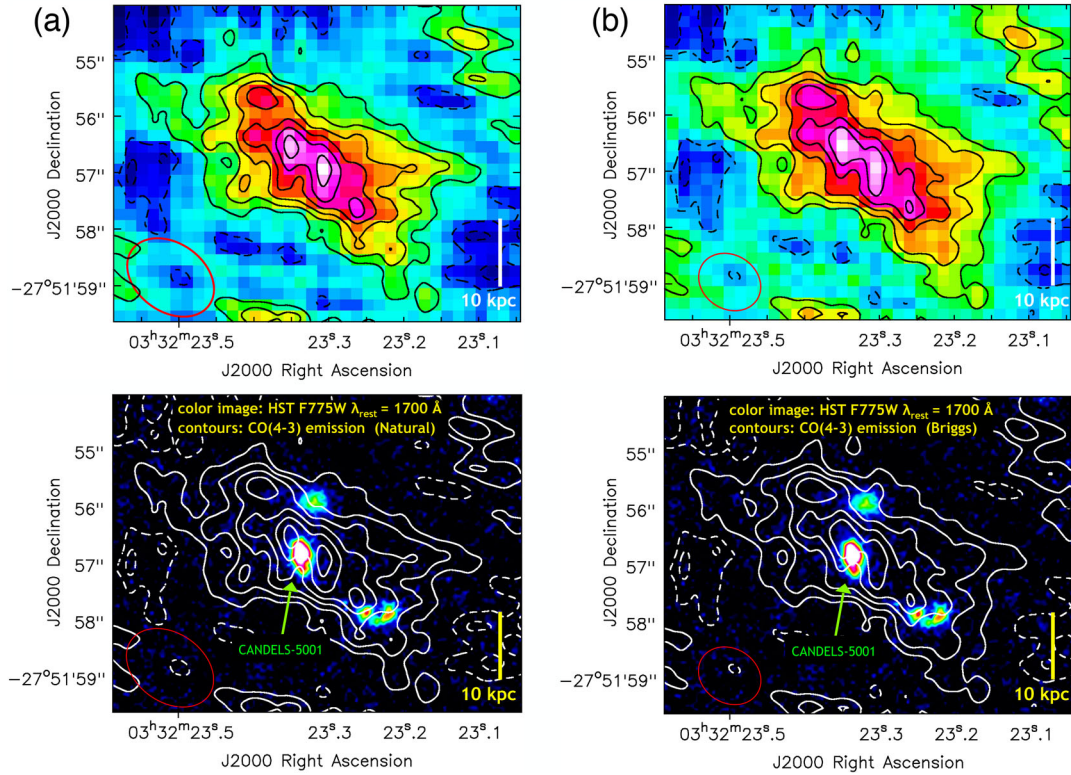
Figure 3. (a) Upper panel: CO J = 4−3 map of the region around Candels-5001 obtained through natural weighting of the visibilities. The CO surface brightness contours range from 1σ to 6σ, where $\sigma = 22\,\mathrm{mJy\,km\,s^{-1}\,beam^{-1}}$ is the CO map rms. Dashed contours indicate negative fluxes. Lower panel: the same CO contours are shown overlaid on to the *F775W HST* image (colour). (b) Upper panel: CO J = 4−3 map obtained through the Briggs weighting (robustness parameter: +2). Contours range from 1σ to 5σ, where $\sigma = 24.5\,\mathrm{mJy\,km\,s^{-1}\,beam^{-1}}$. In this image, the extended emission is even more clearly resolved, over more than 10 independent beams, although the sensitivity is somewhat lower. Lower panel: same background colour image of (a), with surface brightness contours of CO J = 4−3 Briggs weighted map overlaid. The beam sizes of the ALMA maps are given in the bottom-left corners.

4 RESULTS

4.1 Molecular gas structure extending on 40 kpc scale around the central galaxy

A CO J = 4−3 flux map was obtained by collapsing the channels containing line emission ($-140 < v < +140\,\mathrm{km\,s^{-1}}$; see Section 4.2), using a data cube where the CASA natural weight of the visibilities was performed, resulting into the ~ 1.5 arcsec resolution mentioned in Section 3 (specifically beam of 1.6 arcsec × 1.3 arcsec with PA = 54°.32). The resulting CO flux map is shown in Fig. 3a (left-hand panel). The CO emission is clearly extended over about 40 kpc in an elongated structure-oriented NE–SW. In the bottom image of Fig. 3a, the same contours are overlaid on to an optical *Hubble Space Telescope* (*HST*) image (*F775W*), tracing the rest-frame UV emission. We note that the CO map reveals some structures on scales smaller than the beam FWHM; this is a consequence of the presence of some long baselines that provide some sensitivity to small scales and make the beam profile non-Gaussian, as discussed in the previous section.

Fig. 3b shows the same maps obtained with a CASA Briggs weight (i.e. weighting less the more compact baselines), which results into higher angular resolution (beam of 1 arcsec), although at expenses of a somewhat lower sensitivity. The latter image shows even more clearly that the extended emission is fully resolved, over more than 10 independent beams. The flux assigned to Candels-5001 has been estimated collecting the total flux within an ALMA synthesized beam centred on the rest-frame UV emission peak from *HST* images.

Interestingly, although the CO map peaks are associated with the massive star-forming galaxy, Candels-5001 accounts for only about 40 per cent of the CO emission in the central 40 kpc; the remaining CO emission ($\sim$60 per cent) is distributed in the CGM within the elongated structure, and it is not directly associated with either the central target or its two companions.

Within this context, we note that the extended structure cannot be ascribed to molecular gas hosted in the three merging galaxies and 'artificially' smeared on a larger scale by the ALMA beam. This is discussed in more detail in Appendix C through a simple simulation.

We calculated the total molecular mass in the 40 kpc structure traced by the CO J = 4−3 emission, conservatively assuming for such a system the same gas metallicity inferred for the central and nearby galaxies ($\sim 0.5\,\mathrm{Z_\odot}$, e.g. Maiolino et al. 2008, Troncoso et al. 2014, and validated by the Te-based calibration in Curti et al. 2017; this is a conservative assumption as the surrounding gas has probably lower metallicity, although Bouché et al. 2016 have found evidence for inflowing gas with similar metallicity) and using a metallicity-dependent CO-to-H$_2$ conversion factor ($\alpha_{\mathrm{CO}} \sim 10 \pm 2$; Wolfire, Hollenbach & McKee 2010; Feldmann, Gnedin & Kravtsov 2011; Bolatto, Wolfire & Leroy 2013; Saintonge et al. 2013). The inferred total mass of molecular gas within the 40 kpc wide structure is about 2– $6 \times 10^{11}\,\mathrm{M_\odot}$. The given range of gas masses reflects the uncertainty on α_{CO} and on the CO J = 4−3/CO J = 1−0 lines flux ratio, for which we have assumed values ranging from that typically observed in normal (Milky Way-like) star-forming galaxies to that observed in starburst and high-z submillimetre galaxies (Carilli &

**Table 2.** Summary of the properties of the extended molecular gas structure.

Parameter	Global structure $0 < R \lesssim 20\,\text{kpc}$	Extended component $2 < R \lesssim 20\,\text{kpc}$
Line flux CO(4−3) Jy km s^{-1}	0.30 ± 0.05	0.17 ± 0.04
Molecular gas mass $\log(M_{\text{H}_2}/M_\odot)$	$11.60^{+0.18}_{-0.29}$	$11.49^{+0.19}_{-0.28}$
F_{cont}(103 GHz) μJy	75.4 ± 9.6	39.3 ± 9.6
Star formation rate $M_\odot$ yr^{-1}	198 ± 63	103 ± 63

Walter 2013). Table 2 contains detailed information on the extended elongated molecular gas structure surrounding Candels-5001.

It is interesting to note that, as mentioned above, about 40 per cent of this molecular gas is associated with the central galaxy, implying that this is a very gas-rich galaxy ($M_{\text{gas}}/M_\star \sim 6$; Table 1). This is not unprecedented among high-redshift galaxies (e.g. Genzel et al. 2015) and it reveals that this galaxy is in an early evolutionary phase.

4.2 Kinematics properties of the extended gaseous structure

Velocity and velocity dispersion maps of the 40 kpc-scale gaseous structure were obtained by fitting one or two Gaussians to the line profiles and they are shown in the left-hand panels of Fig. 4a. While
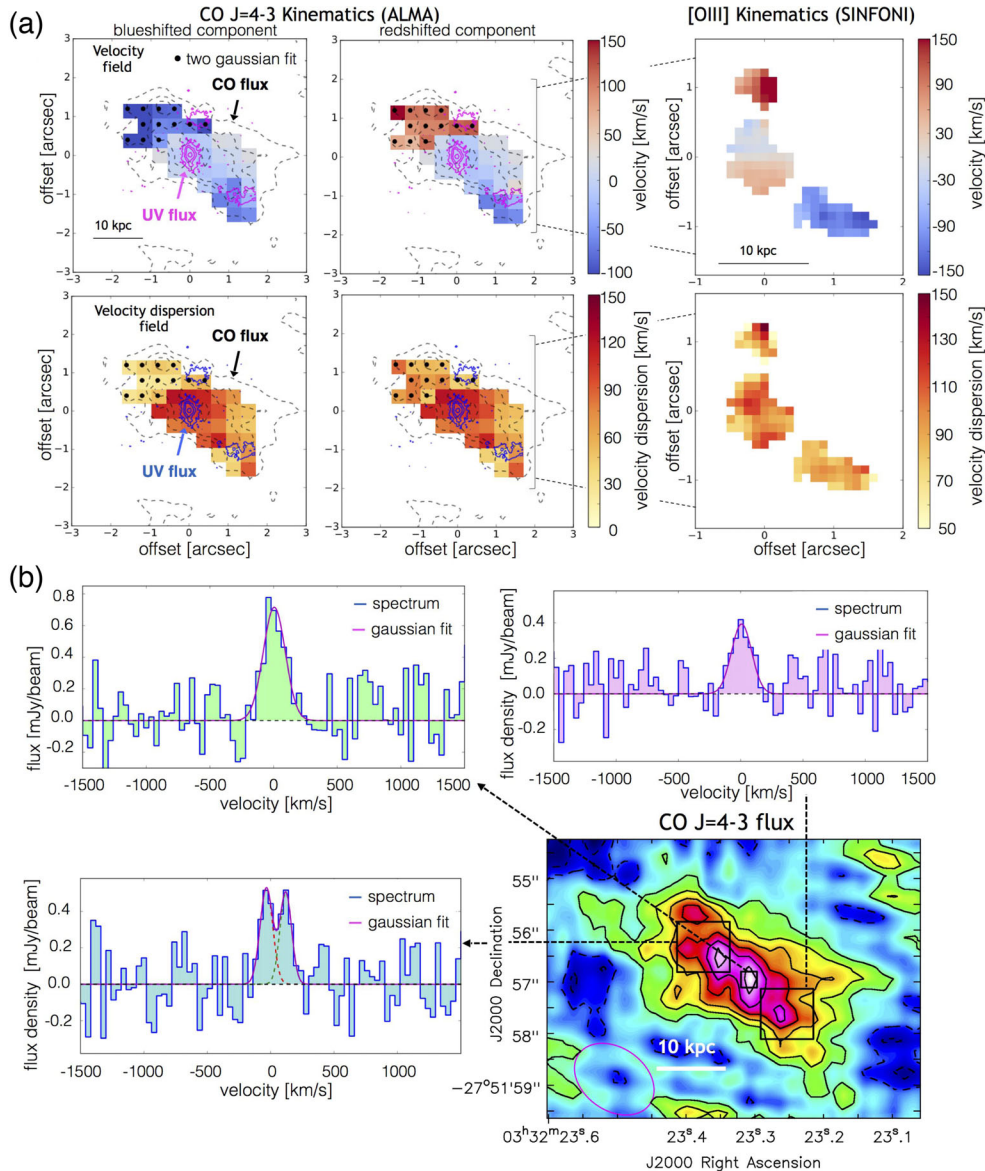
Figure 4. (a) Left-hand panels: CO J = 4−3 velocity field and velocity dispersion. Dots indicate regions where a fit with two Gaussian components is required; in these cases the two kinematics components ('blueshifted' and 'redshifted') are shown separately. The solid contours show the rest-frame UV emission traced by *HST*. Right-hand panels: velocity field and velocity dispersion of the three galaxies traced by the [O III]5007 Å optical nebular emission line (Maiolino et al. 2008; Troncoso et al. 2014). (b) Bottom right panel: CO J = 4−3 surface brightness within the central few tens kpc around Candels-5001 (same levels as Fig. 3a). Top/bottom left panels: spectra extracted from the central region and from two outer regions, one of the latter showing indication of a double-peaked profile.
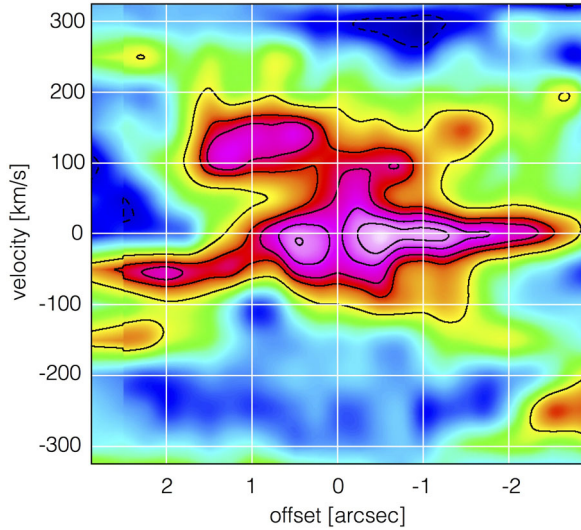
Figure 5. CO J = 4−3 position–velocity diagram along the major axis of the extended structure. The diagram is inconsistent with simple coherent rotation and further showing sub-structures with different velocities at the same location.

Figure 6. Continuum emission at 103 GHz, corresponding to $\lambda_{rest} \sim$ 650 μm. Contours show the surface brightness at 1.5σ, 2.5σ and 3.5σ, where $\sigma = 9.6$ μJy beam^{-1} is the map rms. No negative fluxes at these levels are present in this area.

the overall dynamics broadly follows the velocity distribution of the three optical galaxies (Fig. 4a, right-hand panels), the external region north-west of Candels-5001 appears to be characterized by two different kinematic components. This is clear from the double-peaked profile of the spectrum extracted from the area described above (see the lower left panel of Fig. 4b) and in the position–velocity (p–v) diagram along the major axis (Fig. 5) of the 40 kpc gaseous structure. The regions in which a double-Gaussian fit is required are marked with black dots in Fig. 4a and the kinematics of the two components is shown separately in Fig. 4a (left and central panels).

The p–v diagram does not show any signature of coherent rotation around the massive galaxy. Instead it clearly shows sub-structures with different velocities at the same location. Overall these results highlight an irregular kinematics of the extended elongated molecular structure.

We note that the limited angular resolution of our ALMA data (with respect to the SINFONI observations of Candels-5001) does not allow us to resolve the internal kinematic structure of the molecular gas within the individual galaxies and, in particular, it does not resolve their internal rotation curves that are instead traced by their optical nebular lines (Maiolino et al. 2008) (Fig. 4a, right-hand panels).

The measured CO line velocity dispersion appears to be low, ranging between 30 and 100 km s^{-1} over the entire region (Fig. 4a, lower panels).

4.3 Continuum thermal emission within the 40 kpc extended structure

We detect continuum thermal dust emission (at 103 GHz, corresponding to $\lambda_{rest} \sim 650$ μm) associated with the extended molecular gas structure traced by the CO emission. This is shown in Fig. 6 (with Briggs weighting), illustrating that continuum emission is associated with the central massive galaxy, but also clearly extended along the surrounding structure (without being associated with any of the two companion galaxies).
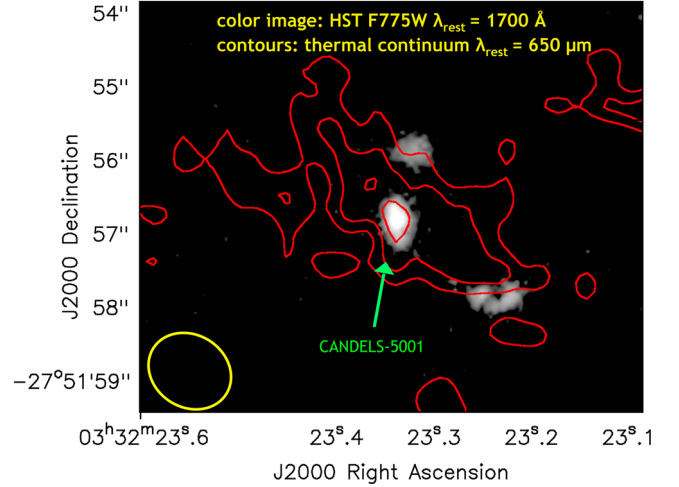
In other works, thermal emission at these wavelengths has been used as a tracer of star formation (whose UV radiation is responsible for heating the dust) and/or as a tracer of the dust mass. Scoville et al. (2014, 2016) have shown that, for most galaxies, in the Rayleigh–Jeans region a constant dust temperature of 25 K can be assumed and, therefore, the continuum emission can be used as a tracer of dust mass. However, this assumption may break down in an extended primordial structure as the one observed by us on 40 kpc scale, both because of the low metallicity and because the ISM may have physical conditions different than in normal galaxies.

We have combined the ALMA continuum detection with the *Herschel* data of the same galaxy. The *Herschel* beam is so large that it is not possible to disentangle the emission on 40 kpc scales from the emission associated with central galaxy Candles-5001. We have therefore performed a fit of the IR-to-millimetre SED of the entire 40 kpc emitting region by using the fitting code CIGALE (Burgarella, Buat & Iglesias-Páramo 2005) to retrieve the main parameters of the system. We obtain that the inferred total star formation rate is 198 ± 63 M$_\odot$ yr^{-1}. This is roughly consistent, although somewhat lower, to the sum of the star formation rates inferred from the optical-UV SED fitting or the (extinction-corrected) Hβ emission of the three merging galaxies, which is about 325 ± 120 M$_\odot$ yr^{-1} (Troncoso et al. 2014). The slightly lower star formation rate (SFR) inferred from the far-IR emission can be explained in terms of lower dust content that absorbs less UV radiation than in metal rich galaxies. From the same fit, we infer a dust mass of $M_{dust} = 1.58$ $(\pm 0.57) \times 10^9$ M$_\odot$. Assuming a metallicity of half solar (as inferred for Candles-5001) and the metallicity-dependent H$_2$-to-dust ratio derived by Leroy et al. (2011), we infer a total molecular mass in the central 40 kpc of $2.1(\pm 0.75) \times 10^{11}$ M$_\odot$, which is roughly consistent with what inferred through the CO emission, within uncertainties (Table 2).

We cannot perform a similar SED analysis on spatially resolved basis due to the low angular resolution of the *Herschel* data. However, to first order, we can assume the same SED fitted to the total IR-to-mm emission and split it into a component associated with Candles-5001 and another one associated with the extended emission ($2 < R < 20$ kpc), with the proportions inferred from the ALMA continuum flux distribution. By using this approach, we infer that
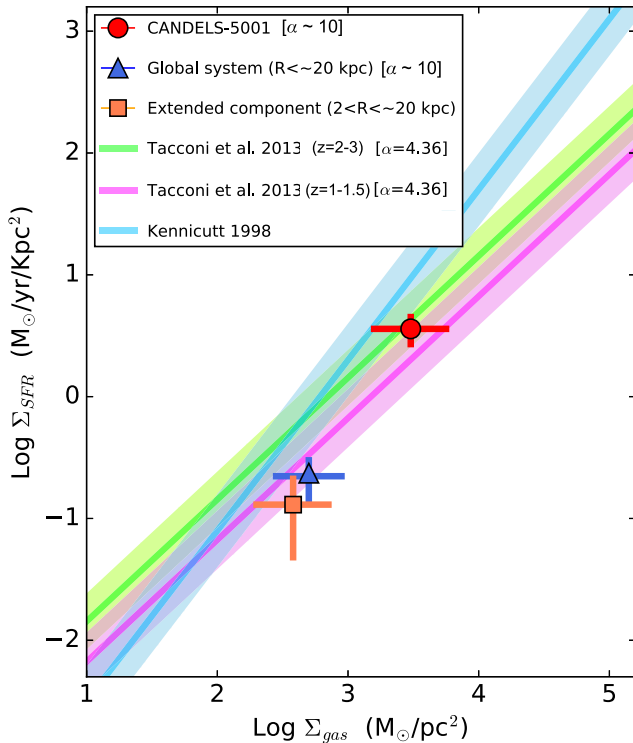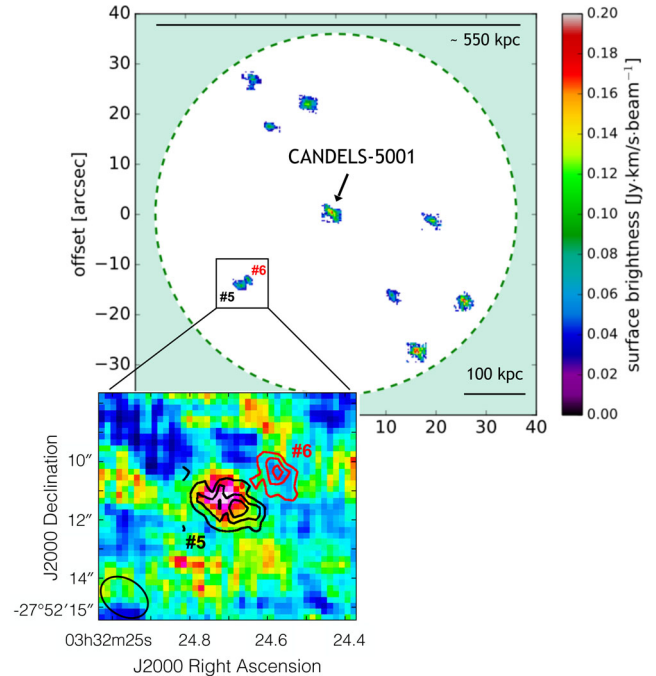
Figure 7. Location of the central massive galaxy and of the 40 kpc extended structure relative to the local and high-z Schmidt–Kennicutt relations between surface density of SFR and surface density of molecular gas.


Figure 8. Distribution of CO-emitting systems detected on the 550 kpc scale around Candels-5001. The dashed circle encloses the region where the primary beam response function is above 30 per cent. The image of each object is shown down to the 1σ level of the CO surface brightness. The inset shows (in colour) the ALMA continuum emission map for the galaxy (in addition to Candels-5001 and its surrounding 40 kpc) clearly detected in continuum. Black and red contours show CO emission systems no. 5 and no. 6 (see Appendix D), respectively, at levels of 2σ, 3.5σ and 5σ.

the SFR in the extended component is $\sim100\,\mathrm{M}_\odot\,\mathrm{yr}^{-1}$. This is similar to the SFR inferred for the central galaxy, but distributed on much larger scales, implying an average surface density of SFR of $0.1\,\mathrm{M}_\odot\,\mathrm{yr}^{-1}\,\mathrm{kpc}^{-2}$. Such extended star formation is not observed in the *HST* rest-frame UV image. From the latter data, we infer an upper limit of $0.03\,\mathrm{M}_\odot\,\mathrm{yr}^{-1}\,\mathrm{kpc}^{-2}$. Such a discrepancy may be ascribed to dust extinction: assuming the dust attenuation curve typical of star-forming galaxies (Calzetti et al. 2000), matching the two observations requires a dust reddening of only $E(B-V) = 0.1$, which is lower than that inferred for the optical star-forming galaxies in the same region (Troncoso et al. 2014). The tentative detection of some weak diffuse emission in longer wavelength *HST* images (*F160W*, tracing continuum stellar emission at $\lambda_{\mathrm{rest}} \sim 3400\,\text{Å}$; see Appendix B) supports such dust-reddening scenario. Alternatively, dust in the extended structure may be significantly cooler than what observed in typical star-forming galaxies, which would imply a significantly lower SFR.

It is interesting to note that, with the Σ_{SFR} inferred above, the 40 kpc extended structure surrounding Candels-5001 is located slightly below (although still marginally consistent with) the Schmidt–Kennicutt relation between SFR and molecular gas (Fig. 7), suggesting that the diffuse star formation in such extended structure is somewhat less efficient than in normal galaxies (Tacconi et al. 2013; Sargent et al. 2014). If a fraction, or most of the continuum emission in the extended structure, is not due to *in situ* star formation, but heated by external optical–UV radiation field, then the inferred star formation efficiency would be even lower.

4.4 Detection of CO systems on 550 kpc scale

We have searched for CO-emitting systems within the ALMA field of view by collapsing spectral channels of the natural weighted data

cube for a resulting channel width ranging from 40 to $200\,\mathrm{km\,s}^{-1}$ (although almost all detections are found with widths larger than $100\,\mathrm{km\,s}^{-1}$) with the centre of the rebinned spectrum spanning the whole waveband, and searching for emission within the area where the primary beam response function is above 30 per cent, i.e. a diameter of ~73 arcsec, corresponding to 550 kpc. Fig. 8 shows the distribution of the CO detections within the ~73 arcsec diameter (traced by the dashed circle) where the colour-coding of the detections gives the surface brightness. The significance of each system was assessed by comparing it with the noise in the map extracted within the same spectral range. To select the reliable CO detections, we used a threshold of 5.2σ for CO peak emission, with the justification that with this threshold the number of negative detections (i.e. the number of sources detected with the same method in the flux-inverted cube) is less than 10 per cent of the positive ones. Indeed, following these criteria, we obtain 10 positive detections and only one negative detection within the spectral window centred on to the CO $J = 4-3$ transition. Moreover, such a negative detection is found at the very edge of the field, as shown in the black box inset of Fig. 9.

This test indicates that the vast majority of the CO systems are not noise fluctuations and that the contamination from spurious detections is only about 10 per cent or less.

Within the other three wavebands, the ratio between positive and negative detections tends to be close to 1, as expected from typical Gaussian noise fluctuations. In such other spectral windows, as a consequence of the higher noise (relative to the band centred on to the CO $J = 4-3$ transition), the number of positive and negative detections is about two or three per spectral band (by using the
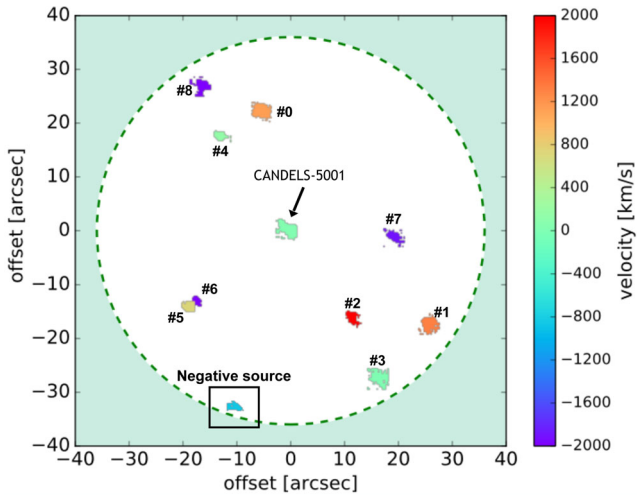
Figure 9. CO-emitting systems colour-coded according to their velocity relative to Candels-5001. Black box: the only negative source (i.e. detected in the inverted flux cube and with the same criteria used to detect the positive sources), in the waveband centred on the CO J = 4−3 transition.

same 'detection criteria' discussed above for CO J = 4−3). Such 'detections' in the other spectral bands (most of which must be associated with noise fluctuations) are isotropically distributed within the field of view.

We note that the field of view does not contain any strong source that may produce prominent side lobes (especially in the narrow bands used for the CO detections).

The zoomed map of each of the CO systems detected on large scales is shown in Fig. 10, along with each individually extracted spectrum.

4.4.1 Physical properties of the ∼550 kpc-scale CO systems

From Fig. 8, it is clear that the CO systems detected on 550 kpc scales are predominately distributed in the same NE–SW direction as the central ∼40 kpc extended molecular gas structure (Fig. 3), strongly suggesting a physical link between them. Assuming metallicities similar to Candels-5001, and using the same calibrators discussed before, we infer for these systems gas masses of about 10^{10}–10^{11} M$_\odot$.

We note that the CO J = 4−3 transition is highly sensitive to the excitation state of the emitting gas, and therefore, since these gas-rich systems may be partially shock-heated (Nelson et al. 2016), this may result into an overestimation of their molecular mass content.

In Appendix D, we show the thumbnails of the optical and near-IR *HST/Spitzer* images of these systems and their properties are also tabulated. Some of the systems show a potential *HST* and/or *Spitzer* counterpart (e.g. systems no. 3 and no. 4), especially if one allows for some offset between ALMA and optical/IR counterparts, which seem to be common among these sources (Dunlop et al. 2017). The ALMA continuum emission is clearly detected in system no. 5 (illustrated in the zoomed inset of Fig. 8), and marginal detections (at the 2.5σ level) are also seen for systems no. 0 and no. 2.

The other systems are not clearly detected individually, however the *HST* stacked image of all CO-emitting sources, shown in Fig. 11, does show a 2.5σ detection. The stacked ALMA continuum emission (excluding system no. 5, which is individually detected) results into a 3σ detection (Fig. 11). Unfortunately, given the lack of information at other IR wavelengths, we cannot directly translate this flux (∼ 11 μJy) into SFR or dust mass. Yet, if we assume the same SED

as the central region, then the implied average SFR of these systems would be about 30 M$_\odot$ yr^{-1}. Interestingly, a 3σ detection is also obtained by the stacked *Chandra*/ACIS X-ray image (0.5–8 keV), as shown in Fig. 11. The stacked flux is consistent (Ranalli, Comastri & Setti 2003) with the X-ray emission expected from galaxies with an average SFR in the range of 50–120 M$_\odot$ yr^{-1} (depending on whether the soft X-ray relation or the hard X-ray relation of Ranalli et al. 2003 is used and also depending on the assumed X-ray slope). It is interesting to note that such SFR, combined with the average molecular gas mass inferred for these systems (∼ 1.5×10^{11} M$_\odot$), would imply that these systems have an average depletion time of 2 Gyr, i.e. are less efficient in forming stars than normal (main-sequence) galaxies at the redshift of the source (Sargent et al. 2014). If some of the X-ray flux is contributed by obscured AGNs and/or if we take the SFR inferred from the stacked thermal continuum emission discussed above, then their depletion time-scale would be even longer.

The velocity map of the CO systems on a large scale, relative to Candels-5001 and its surrounding molecular gas (Fig. 9), shows that they uniformly cover the ALMA waveband, ranging velocities from few hundred km s^{-1} up to almost ±2000 km s^{-1}.

Some of the high-velocity systems may be affected by the local environment and their velocity could be boosted as a consequence of close gravitational interactions. This is clearly the case for the low-mass, high-velocity CO system no. 6, located a few arcsec from the more massive galaxy no. 5. The former is probably a satellite galaxy in the process of merging with the more massive nearby galaxy companion, and its peculiar high velocity may simply be the result of the local merging process.

We note that the high-velocity spread of the large-scale CO systems is comparable with the velocity dispersions observed in other high-*z* protoclusters (Casey et al. 2015; Chiang et al. 2015), and indeed it is consistent with the redshift range ($\Delta z \sim 0.015$) of the peak in the redshift distribution of the spectroscopically identified galaxies in the GOODS-S field (Fig. 1).

Therefore, the high-velocity CO emitters may be actually tracing the gravitational field of the forming protocluster. Fig. 12 shows the three-dimensional distribution of the CO systems identified in the ALMA field of view (blue symbols), along with the distribution of the spectroscopically identified optical galaxies (magenta symbols) in GOODS-S, further confirming that all those objects in this narrow redshift interval belong to a protocluster, traced by an overdense region spanning a few Mpc in size.

5 DISCUSSION

Previous observations of CO rotational transitions at high-*z* have found molecular gaseous structures, in some cases quite extended, on scales of even about 10 kpc (Hodge et al. 2012; Tacconi et al. 2013; Decarli et al. 2016). Such systems have generally been interpreted as large rotating gaseous discs, in which optical clumps are identified as regions of star formation occurring within such discs (Genzel et al. 2011). Relatively large discs have also been identified in the ionized gas component, through H α imaging (Genzel et al. 2006, 2010, 2014); the latter is mostly a proxy of star formation and probes only a very small fraction (the warm ionized phase) of the gas content in galaxies.

Differently from these objects, our observations of the extended (∼40 kpc) elongated molecular gas structure surrounding Candels-5001 cannot be interpreted in terms of a single large gaseous rotating galaxy disc, in which the optically identified galaxies are sub-clumps. In the following text, we describe the main
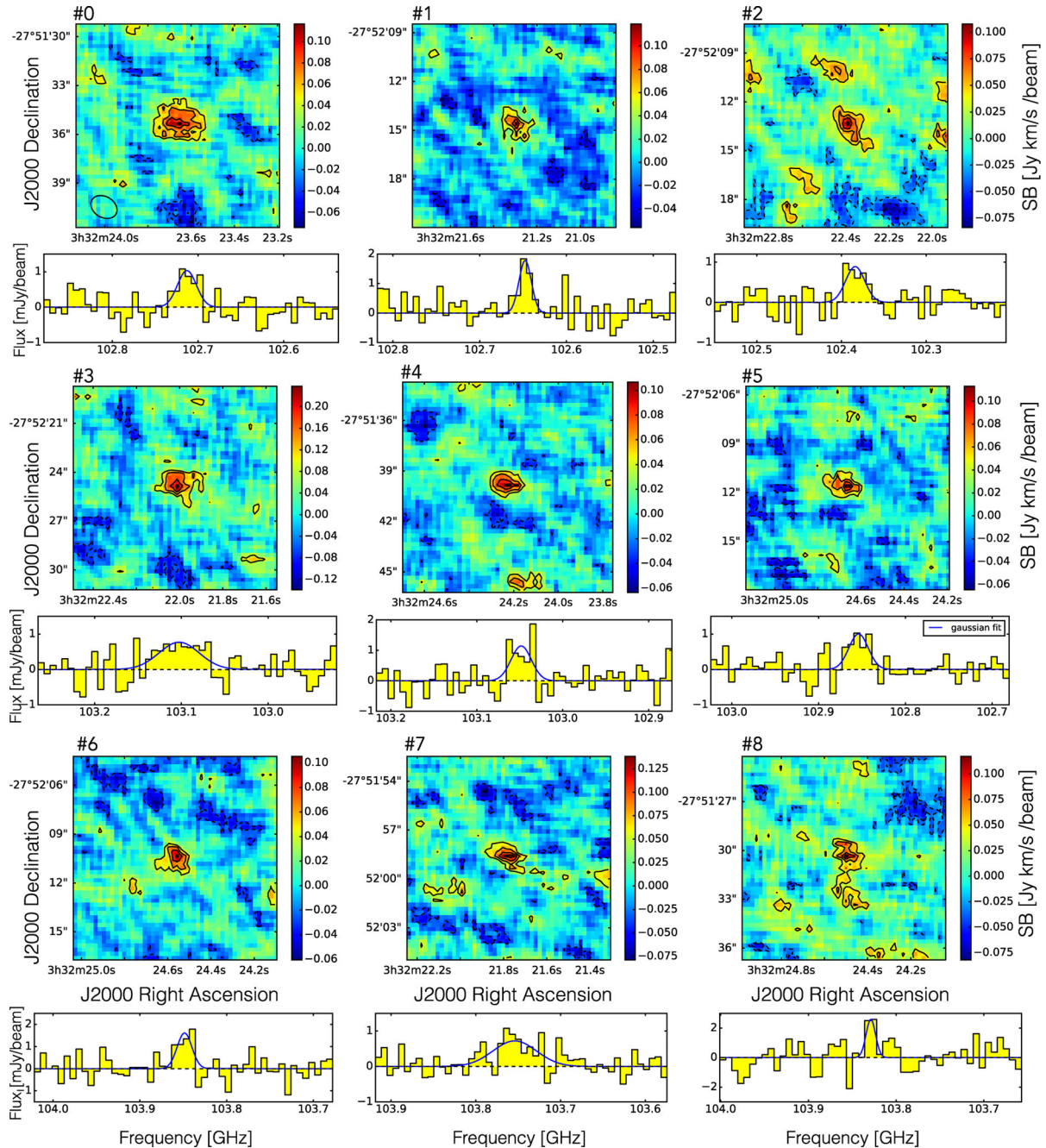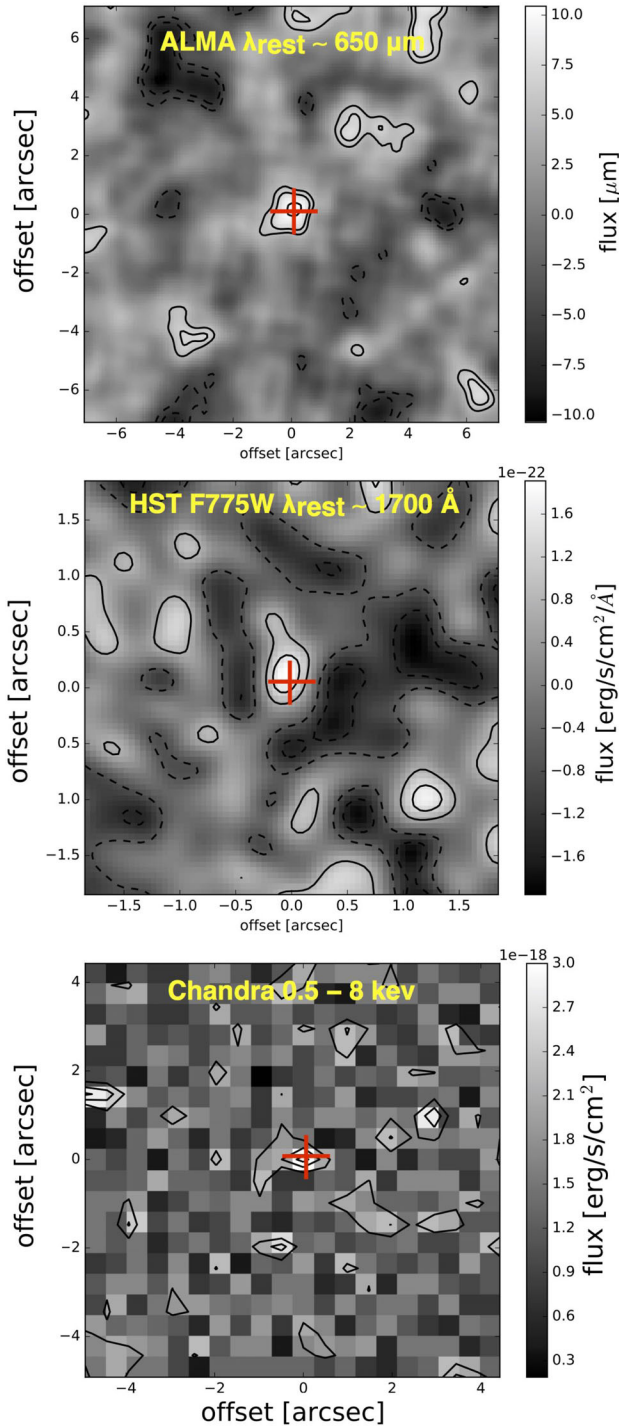
Figure 10. CO J = 4−3 maps of the individual systems detected on large scales, along with their spectra. CO surface brightness contours are shown, at levels of 2σ, 3σ, 4σ, 5σ, where σ is the rms in each CO map. Dashed contours indicate negative fluxes. The beam size of the maps is given in the bottom-left corner of the upper-left panel.

inconsistencies with such a scenario. First, we note that molecular galaxy discs as large as 40 kpc have never been observed and have not been expected by any theory or cosmological simulation, especially at $z > 3$ (the largest putative molecular disc found so far has a size of ~ 20 kpc, reported by Tacconi et al. 2013, and it is at $z \sim 1.2$, i.e. at a much later cosmic epoch). Even more importantly, as traced by the [O III]5007 Å optical nebular line (SINFONI observations; Fig. 4a), the individual optical systems (Candels-5001 and its two companions) have individually resolved rotation curves, which are inconsistent with the interpretation of them being sub-clumps of
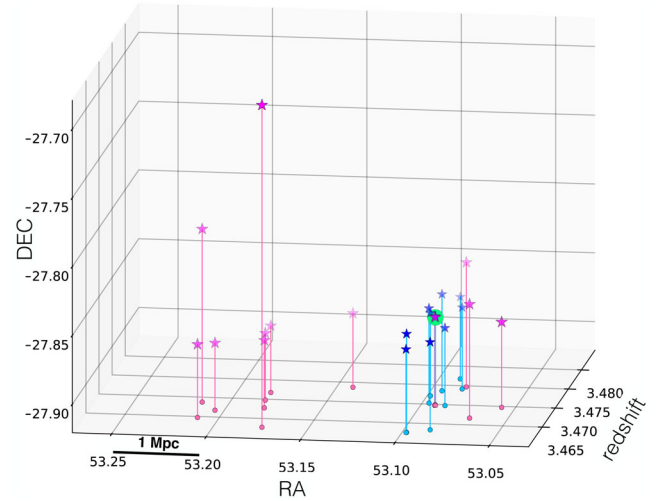
a single very massive galaxy disc. Finally, and most importantly, as already shown in Section 4.2 the CO position–velocity diagram along the major axis (Fig. 5) is completely inconsistent with a single large coherently rotating disc.

An alternative scenario in which the observed extended CO emission is tracing tidally stripped molecular gas is also not plausible. It would imply that the fraction of molecular gas mass stripped out of the galaxy by gravitational interactions with the two satellites would exceed 60 per cent. In contrast to the atomic gas phase (which is located primarily in the galaxy outskirts and more loosely bound),

Figure 12. Distribution of the galaxies spectroscopically identified in the redshift spike shown in Fig. 1 (magenta symbols), along with the distribution of the CO systems (blue symbols) in the right ascension–declination–redshift diagram. The location of Candels-5001 is indicated with a green circle.

Figure 11. Upper panel: the ALMA continuum stacked image of the large-scale CO emitters (excluding system no. 5, which is individually detected). Contours levels: 1σ, 2σ, 3σ. Central panel: *HST F775W* stacked image of all CO sources on large scales. Contours levels: 1σ, 2σ. Lower panel: *Chandra*/ACIS X-ray stacked image of all CO sources. Contours levels: 1σ, 2σ, 3σ.

the molecular gas phase in galaxies is more centrally concentrated and more gravitationally bound. Indeed, both observations and simulations show that, in merging/interacting galaxies, only a tiny fraction, if any, of the molecular gas goes in tidal tails, while the bulk of the molecular gas becomes even more centrally concentrated,

as a consequence of angular momentum losses due to cloud–cloud collisions (Sanders & Mirabel 1996; Narayanan et al. 2006; Ueda et al. 2014).

We also discard the possibility of the massive gas reservoir surrounding Candels-5001 being the product of starburst or stellar-feedback driven outflows. The huge amount of mass found in the gaseous structure around Candels-5001 ($M_{\rm gas} \sim 1.5$–4.5×10^{11} M$_\odot$, see Table 2) and the low CO line velocity dispersion ($\lesssim 100$ km s^{-1}; lower panels of Fig. 4a) are indeed inconsistent with systems where such phenomena really occur, indicating that the extended structure is not associated with a molecular outflow. Within this context, it is also important to note that, as mentioned in Section 2, Fiore et al. (2012) excluded any possible AGN activity in Candles-5001, hence further discarding the scenario of a powerful AGN-driven outflow.

5.1 Molecular gas in accreting streams

We suggest that our ALMA observations of the extended ($\sim$40 kpc) elongated gaseous structure surrounding Candels-5001, combined with its kinematic properties and the overdense environment, are consistent with the system tracing the inner and densest parts of large-scale filamentary streams, feeding the central massive galaxy.

The different kinematic components within such extended structure, identified in both the velocity field (Fig. 4a) and the *p*–*v*-diagram (Fig. 5), indicate that Candels-5001 is likely at the convergence point of three intersecting filaments, as models predict for early massive galaxies (Keres et al. 2005; Dekel et al. 2009; van de Voort et al. 2011; Shen et al. 2013; Sánchez Almeida et al. 2014; Nelson et al. 2016).

If this interpretation is correct, then this would be one of the very first evidences of molecular gas accreting onto a massive galaxy in the early Universe, as well as the first detection of the gas reservoirs supposed to surround high-redshift objects in terms of their molecular phase, which traces the most massive component.

MRC 1138-262, often referred as the 'Spiderweb Galaxy' (Pentericci et al. 2002; Miley et al. 2006; Nesvadba et al. 2006;

Venemans et al. 2007), a radio galaxy at the centre of a protocluster, could be another system in which accretion of cold gas may be occurring, although at a significantly lower redshift ($z = 2.16$) than Candels-5001. However, observational evidence for cold accretion in this system is still unclear or marginal. Indeed, observations of molecular gas of this system have either been at very low angular resolution (9.5×5.3 arcsec $= 80 \times 45$ kpc; Emonts et al. 2013), preventing the association of the molecular emission with intracluster molecular gas or with the blending of CO emission from the various merging galaxies optically identified within the beam of the radio observation, or resulted in the detection of a few individual clumps associated with either AGN nuclei or clumps excited by the radio jets produced by the central radio galaxy (Gullberg et al. 2016).

Our detection is likely resulting from a combination of several factors, specifically (1) sensitivity enabled by ALMA; (2) instrument configuration (enabling the detection of diffuse/extended emission on large scales); (3) properly selected target at the proper cosmic epoch (a massive galaxy at the centre of a protocluster, at redshift $z = 3.47$, when accretion from cosmic streams is expected to be particularly prominent and not yet significantly disrupted by halo-induced shocks); (4) observation of a high enough transition, CO J $= 4-3$, which does not suffer from the reduced contrast against the cosmic microwave background (CMB) (warmer by a factor of $1 + z$), which may prevent the detection of very extended emission in lower CO transitions observations (Zhang et al. 2016).

Our interpretation is further supported by the detection of gas-rich systems on even larger scales, $\sim$550 kpc, predominantly distributed in the same direction as the central 40 kpc elongated structure (Section 4.4). The inferred mass of such CO emitters is in the range of that estimated for gas-rich protogalaxies expected to form in cosmic filaments according to simulations (Dekel et al. 2009; Nelson et al. 2016). Therefore, we suggest that some of the detected gaseous systems (especially those with velocities within a few hundred km s^{-1}, consistent with them being gravitationally associated with the 40 kpc scale gaseous structure) may be tracing the same filamentary streams terminating onto the central massive galaxy and producing the inner elongated condensation of molecular gas.

Large molecular gas masses within filamentary accreting gas structures, traced by CO, indicate the presence of past and ongoing star formation in such streams, which has resulted in some pre-enrichment even before they enter the massive galaxies discs. As mentioned in the Introduction section, such pre-enrichment of cold gaseous streams, due to gravitational collapse and star formation along the accreting filaments, eventually leading protogalaxies formation, is expected by cosmic simulations (Dekel et al. 2009; Darvish et al. 2014; Nelson et al. 2015, 2016; Ceverino et al. 2016). This scenario is further confirmed by the observation of ongoing star formation in the 40 kpc extended CO molecular structure and in the 550 kpc-scale CO systems that are associated with the stream (through either individual detections or stacking). In this light, also the two optical companion galaxies of Candels-5001 may be the result of such fragmentation and star formation occurred along the filaments.

One potential concern is that studies attempting to trace cold streams through absorption along the line of sight of quasars have pointed at very low metallicities (e.g. Fumagalli, O'Meara & Prochaska 2016). However, these studies have generally identified absorption systems around less massive galaxies. Moreover, even in massive galaxies, it is expected that the filling factor of dense (enriched) molecular systems along the streams is low, hence the chance of detecting them through random lines of sights probed by background quasars is very low. It is however interesting to note that some studies, exploiting the analysis of absorption systems in the vicinity of high-redshift galaxies, have indeed found evidence of gas in accretion with relatively high metallicities ($\sim$0.4 Z$_\odot$; Bouché et al. 2013, 2016).

6 CONCLUSIONS

We have presented the ALMA observations targeting the field of Candels-5001, the most massive galaxy ($M_\star = 1.9 \times 10^{10}$ M$_\odot$) in the redshift range $3 < z < 4$ within the GOODS-S field. This galaxy lies in an overdense region (located in a prominent redshift spike), likely tracing a forming protocluster (Franck & McGaugh 2016). Taking advantage of such overdense environment, expected to more efficiently enrich the intergalactic environment, we investigated the molecular gas distribution traced by the ALMA observations of the CO J $= 4-3$ rotational transition.

Our findings can be summarized as follows.

(i) We detect a large structure of molecular gas reservoir around Candels-5001, extended over 40 kpc with a clearly elongated morphology (Fig. 3).

(ii) By using a metallicity dependent CO-to-H$_2$ conversion factor (Bolatto et al. 2013) and a range of values for the CO J $= 4-3$/CO J $= 1-0$ lines flux ratio (Carilli & Walter 2013), we infer for the gaseous structure a mass of $M_{gas} \sim 2-6 \times 10^{11}$ M$_\odot$. About 60 per cent of the mass is not directly associated with either the central galaxy or its two satellites, but is distributed in the IGM in the vicinity of the central galaxy. Such large amount of molecular mass in the CGM cannot be explained in terms of tidally stripped molecular gas due to gravitational interaction (see Section 5).

(iii) The molecular gas in the central 40 kpc has a complex kinematics. The north-east external region of the gaseous structure appears to be characterized by two distinct kinematic components (Fig. 4). The p–v diagram does not show any signature of coherent rotation of the large structure, instead showing sub-structures with different velocities at the same location (Fig. 5). As traced by the [O III]5007 Å optical nebular lines, Candels-5001 and its two companions have individually resolved rotation curves. Altogether these kinematics evidences rule out the scenario in which the detected molecular structure is tracing a large rotating disc where the individual optical systems are sub-clumps.

(iv) We detect continuum thermal dust emission ($\lambda_{rest} \sim 650\,\mu$m) associated with the CO structure on 40 kpc scales. Together with the *Herschel* data, the IR-to-mm continuum SED indicates a dust mass of about 1.6×10^9 M$_\odot$. Using a dust-to-gas conversion factor appropriate for the metallicity in this system, this dust mass corresponds to a gas mass of about 2×10^{11} M$_\odot$, consistent with that inferred from CO observations.

(v) The extended continuum emission also suggests that the extended structure is undergoing star formation at a rate of about 0.1 M$_\odot$ yr^{-1}kpc^{-2} or lower. This indicates that star formation in the extended structure is close to the Schmidt–Kennicutt relation (Fig. 7), but slightly less efficient than in normal star-forming galaxies at this redshift.

(vi) We detect gas-rich systems on scales of $\sim$500 kpc, within the ALMA field of view, most of which are distributed in the same NE–SW direction as the central CO $\sim$ 40 kpc elongated structure (Fig. 8). Assuming metallicities similar to Candels-5001, and using the same calibrators discussed before, we infer for these systems gas masses of about 10^{10}–10^{11} M$_\odot$.

(vii) Some of the systems have individual ALMA continuum detections. The other systems are detected in the stacked ALMA continuum map and also in the stacked X-ray image. They are also marginally detected (2.5σ) at optical wavelength in the stacked *HST* image (UV restframe). Their inferred average SFR (about 30–120 $M_\odot$ yr^{-1}), compared with their average content of molecular gas, indicates that these systems are less efficient in forming stars than normal galaxies at this redshift (average depletion time-scales of 2 Gyr or longer).

(viii) The velocity spread of the large-scale CO systems, relative to Candels-5001, is comparable with the velocity dispersions observed in other high-z protoclusters (Casey et al. 2015; Chiang et al. 2015), indicating that these systems may be tracing the gravitational field of the forming protocluster.

We suggest that the 40 kpc extended CO emission, combined with the kinematics analysis, showing the presence of different kinematics components, is consistent with the system tracing the inner part of large-scale accreting streams, feeding the central massive galaxy. Our interpretation is corroborated by the CO-emitting systems detected up to a distance of $\sim$250 kpc from the galaxy (in the ALMA field of view), whose distribution is aligned with the inner 40 kpc gaseous structure. Some of these objects may be tracing the densest regions of the same filamentary streams terminating onto the massive galaxy.

The detected continuum thermal dust emission associated with the accreting structure on the 40 kpc scale, as well as the X-ray, optical and millimetre emission detected in the CO systems on large scales, indicates that a fraction of gas in the streams undergoes star formation (although inefficiently) even before accreting onto the central galaxy.

These findings are in agreement with several cosmological models of galaxy formation and evolution at early epochs, according to which cosmic gaseous streams feeding massive galaxies are clumpy and may undergo gravitational collapse, by forming stars and protogalaxies, hence enriching a fraction of the gas in the streams, even before accreting onto the massive galaxy (Dekel et al. 2009; Kereš et al. 2009; Pallottini et al. 2014; Sánchez Almeida et al. 2014; Ceverino et al. 2016; Nelson et al. 2016).

ACKNOWLEDGEMENTS

REFERENCES

Birnboim Y., Dekel A., 2003, MNRAS, 345, 349
Bolatto A. D., Wolfire M., Leroy A. K., 2013, ARA&A, 51, 207
Borisova E. et al., 2016, ApJ, 831, 39
Bouché N., Murphy M. T., Kacprzak G. G., Péroux C., Contini T., Martin C. L., Dessauges-Zavadsky M., 2013, Science, 341, 50
Bouché N. et al., 2016, ApJ, 820, 121
Brooks A. M., Governato F., Quinn T., Brook C. B., Wadsley J., 2009, ApJ, 694, 396
Bunker A. J., Marleau F. R., Graham J. R., 1998, AJ, 116, 2086
Burgarella D., Buat V., Iglesias-Páramo J., 2005, MNRAS, 360, 1413
Calzetti D., Armus L., Bohlin R. C., Kinney A. L., Koornneef J., Storchi-Bergmann T., 2000, ApJ, 533, 682
Cantalupo S., Porciani C., Lilly S. J., Miniati F., 2005, ApJ, 628, 61
Cantalupo S., Lilly S. J., Haehnelt M. G., 2012, MNRAS, 425, 1992
Cantalupo S., Arrigoni-Battaia F., Prochaska J. X., Hennawi J. F., Madau P., 2014, Nature, 506, 63
Carilli C. L., Walter F., 2013, ARA&A, 51, 105
Casey C. M. et al., 2015, ApJ, 808, L33
Cattaneo A., Dekel A., Devriendt J., Guiderdoni B., Blaizot J., 2006, MNRAS, 370, 1651
Ceverino D., Sánchez Almeida J., Muñoz Tuñón C., Dekel A., Elmegreen B. G., Elmegreen D. M., Primack J., 2016, MNRAS, 457, 2605
Chiang Y.-K. et al., 2015, ApJ, 808, 37
Curti M., Cresci G., Mannucci F., Marconi A., Maiolino R., Esposito S., 2017, MNRAS, 465, 1384
Darvish B., Sobral D., Mobasher B., Scoville N. Z., Best P., Sales L. V., Smail I., 2014, ApJ, 796, 51
Decarli R. et al., 2016, ApJ, 833, 70
Dekel A., Birnboim Y., 2006, MNRAS, 368, 2
Dekel A. et al., 2009, Nature, 457, 451
Dunlop J. S. et al., 2017, MNRAS, 466, 861
Emonts B. H. C. et al., 2013, MNRAS, 430, 3465
Fall S. M., Efstathiou G., 1980, MNRAS, 193, 189
Feldmann R., Gnedin N. Y., Kravtsov A. V., 2011, ApJ, 732, 115
Fiore F. et al., 2012, A&A, 537, A16
Franck J. R., McGaugh S. S., 2016, ApJ, 817, 158
Fraternali F., 2014, in Feltzing S., Zhao G., Walton N. A., Whitelock P., eds, Proc. IAU Symp. Vol. 298, Setting the scene for Gaia and LAMOST. Cambridge Univ. Press, Cambridge, p. 228
Fumagalli M., O'Meara J. M., Prochaska J. X., 2016, MNRAS, 455, 4100
Geach J. E. et al., 2009, ApJ, 700, 1
Genel S. et al., 2012, ApJ, 745, 11
Genzel R. et al., 2006, Nature, 442, 786
Genzel R. et al., 2010, MNRAS, 407, 2091
Genzel R. et al., 2011, ApJ, 733, 101
Genzel R. et al., 2014, ApJ, 785, 75
Genzel R. et al., 2015, ApJ, 800, 20
Grazian A. et al., 2006, A&A, 449, 951
Gullberg B. et al., 2016, A&A, 591, A73
Haardt F., Madau P., 1996, ApJ, 461, 20
Hennawi J. F., Prochaska J. X., Cantalupo S., Arrigoni-Battaia F., 2015, Science, 348, 779
Hodge J. A., Carilli C. L., Walter F., de Blok W. J. G., Riechers D., Daddi E., Lentati L., 2012, ApJ, 760, 11
Kereš D., Katz N., Weinberg D. H., Davé R., 2005, MNRAS, 363, 2
Kereš D., Katz N., Fardal M., Davé R., Weinberg D. H., 2009, MNRAS, 395, 160
Kollmeier J. A., Zheng Z., Davé R., Gould A., Katz N., Miralda-Escudé J., Weinberg D. H., 2010, ApJ, 708, 1048
Leroy A. K. et al., 2011, ApJ, 737, 12
Lowenthal J. D., Hogan C. J., Leach R. W., Schmidt G. D., Foltz C. B., 1990, ApJ, 357, 3
McMullin J. P., Waters B., Schiebel D., Young W., Golap K., 2007, in Shaw R. A., Hill F., Bell D. J., eds, ASP Conf. Ser. Vol. 376, Astronomical Data Analysis Software and Systems XVI. Astron. Soc. Pac., San Francisco, p. 127
Maiolino R. et al., 2008, A&A, 488, 463
Maiolino R. et al., 2015, MNRAS, 452, 54
Matteucci F., 2014, The Origin of the Galaxy and Local Group, Saas-Fee Advanced Course, Vol. 37. Springer, Berlin, p. 145

Matteucci F., Francois P., 1989, MNRAS, 239, 885

Miley G. K. et al., 2006, ApJ, 650, L29

Narayanan D. et al., 2006, ApJ, 642, L107

Nelson D., Genel S., Vogelsberger M., Springel V., Sijacki D., Torrey P., Hernquist L., 2015, MNRAS, 448, 59

Nelson D., Genel S., Pillepich A., Vogelsberger M., Springel V., Hernquist L., 2016, MNRAS, 460, 2881

Nesvadba N. P. H., Lehnert M. D., Eisenhauer F., Gilbert A., Tecza M., Abuter R., 2006, ApJ, 650, 693

Ocvirk P., Pichon C., Teyssier R., 2008, MNRAS, 390, 1326

Pallottini A., Gallerani S., Ferrara A., 2014, MNRAS, 444, L105

Pallottini A., Ferrara A., Gallerani S., Vallini L., Maiolino R., Salvadori S., 2017, MNRAS, 465, 2540

Patrício V. et al., 2016, MNRAS, 456, 4191

Pentericci L., Kurk J. D., Carilli C. L., Harris D. E., Miley G. K., Röttgering H. J. A., 2002, A&A, 396, 109

Prochaska J. X., Lau M. W., Hennawi J. F., 2014, ApJ, 796, 140

Ranalli P., Comastri A., Setti G., 2003, A&A, 399, 39

Rees M. J., Ostriker J. P., 1977, MNRAS, 179, 541

Saintonge A. et al., 2013, ApJ, 778, 2

Sánchez Almeida J., Elmegreen B. G., Muñoz-Tuñón C., Elmegreen D. M., 2014, A&AR, 22, 71

Sancisi R., Fraternali F., Oosterloo T., van der Hulst T., 2008, A&AR, 15, 189

Sanders D. B., Mirabel I. F., 1996, ARA&A, 34, 749

Santini P. et al., 2009, A&A, 504, 751

Santini P. et al., 2015, ApJ, 801, 97

Sargent M. T. et al., 2014, ApJ, 793, 19

Scoville N. et al., 2014, ApJ, 783, 84

Scoville N. et al., 2016, ApJ, 820, 83

Shen S., Madau P., Guedes J., Mayer L., Prochaska J. X., Wadsley J., 2013, ApJ, 765, 89

Silk J., Mamon G. A., 2012, Res. Astron. Astrophys., 12, 917

Stewart K. R., Kaufmann T., Bullock J. S., Barton E. J., Maller A. H., Diemand J., Wadsley J., 2011, ApJ, 738, 39

Tacconi L. J. et al., 2013, ApJ, 768, 74

Tinsley B. M., 1981, ApJ, 250, 758

Troncoso P. et al., 2014, A&A, 563, A58

Ueda J. et al., 2014, ApJS, 214, 1

van de Voort F., Schaye J., Booth C. M., Haas M. R., Dalla Vecchia C., 2011, MNRAS, 414, 2458

Vanzella E. et al., 2017, MNRAS, 465, 3803

Venemans B. P. et al., 2007, A&A, 461, 823

White S. D. M., Rees M. J., 1978, MNRAS, 183, 341

Wisotzki L. et al., 2016, A&A, 587, A98

Wolfire M. G., Hollenbach D., McKee C. F., 2010, ApJ, 716, 1191

Zhang Z.-Y., Papadopoulos P. P., Ivison R. J., Galametz M., Smith M. W. L., Xilouris E. M., 2016, R. Soc. Open Sci., 3, 160025

APPENDIX A: ASTROMETRIC ALIGNMENT

We have noticed that a systemic offset of about 0.5 arcsec in the same direction is revealed between the optical image of Candels-5001 and the peak of the ALMA continuum emission, as well as between the image of a low-redshift galaxy in the ALMA field of view (COMBO17-25370, MUSIC ID 04383) and the serendipitous detection of an emission line associated with the same galaxy (most likely CO J = 2−1 at z=1.2). Fig. A1 shows the optical *HST* images of Candles-5001 (top) and of the serendipitous foreground galaxy COMBO17-25370 (bottom) overlay on to the ALMA continuum emission (top) and the CO J = 2−1 transition of the serendipitous galaxy (bottom), illustrating that they are indeed subject to the same offset in the same direction.

As discussed in Section 3, this kind of systemic offset has been identified in other studies comparing ALMA and optical data, and is ascribed to astrometric uncertainties associated with the optical
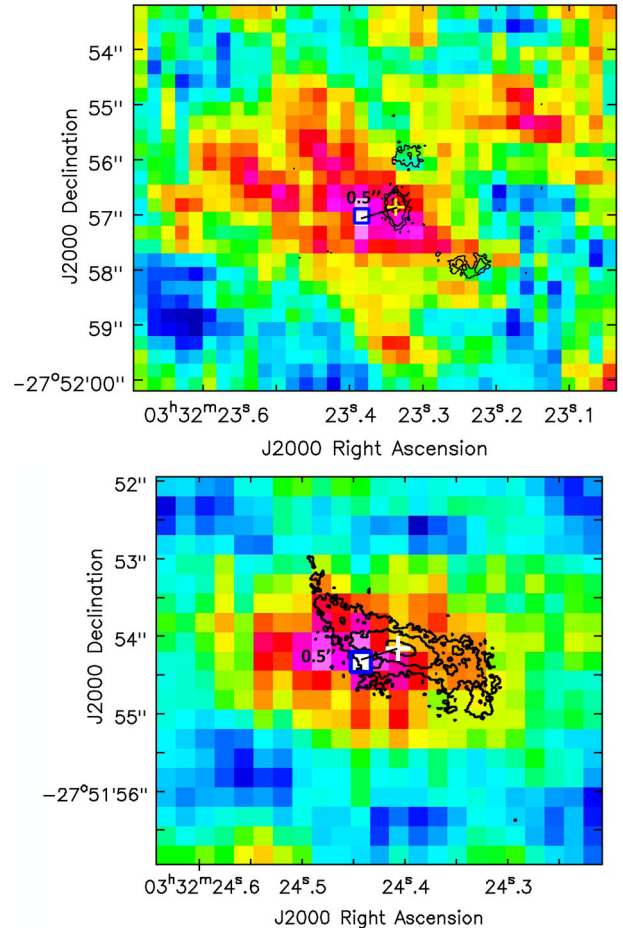
Figure A1. Astrometric shift. Top panel: optical *HST* image (contour) overlaid on to the ALMA continuum image (colour) of Candels-5001. Bottom panel: optical image of a foreground galaxy (COMBO17-25370, contours) overlaid on to its CO(2−1) emission serendipitously detected by ALMA (colour) within the field of view of Candels-5001. In both images, the white cross indicates the peak of the optical emission while the blue square indicates the peak of the ALMA map. Clearly, in both cases, there is a systemic offset of 0.5 arcsec between the optical and millimetre images in the same direction, indicative of an astrometric shift to be corrected.

images, or with the ALMA phase calibrator, or both of them. As a consequence, we performed a slight astrometric alignment of ~0.5 arcsec in the NW direction, to match the ALMA data with the optical images. However, even if neglected, such alignment would not affect the conclusions of the paper.

APPENDIX B: MULTIBAND IMAGES OF CANDELS-5001

In Fig. B1, we show the overlay of the CO(4–3) map with all available *HST* images, as well as with the 3.6 μm *Spitzer* image. The rest-frame wavelength corresponding to each image is indicated in each panel. The tentative detection of some weak diffuse emission in the *HST F*160*W* images, tracing continuum stellar emission at $\lambda_{rest} \sim 3400$ Å, supports the scenario in which some dust-reddening is affecting the low surface brightness star formation occurring in
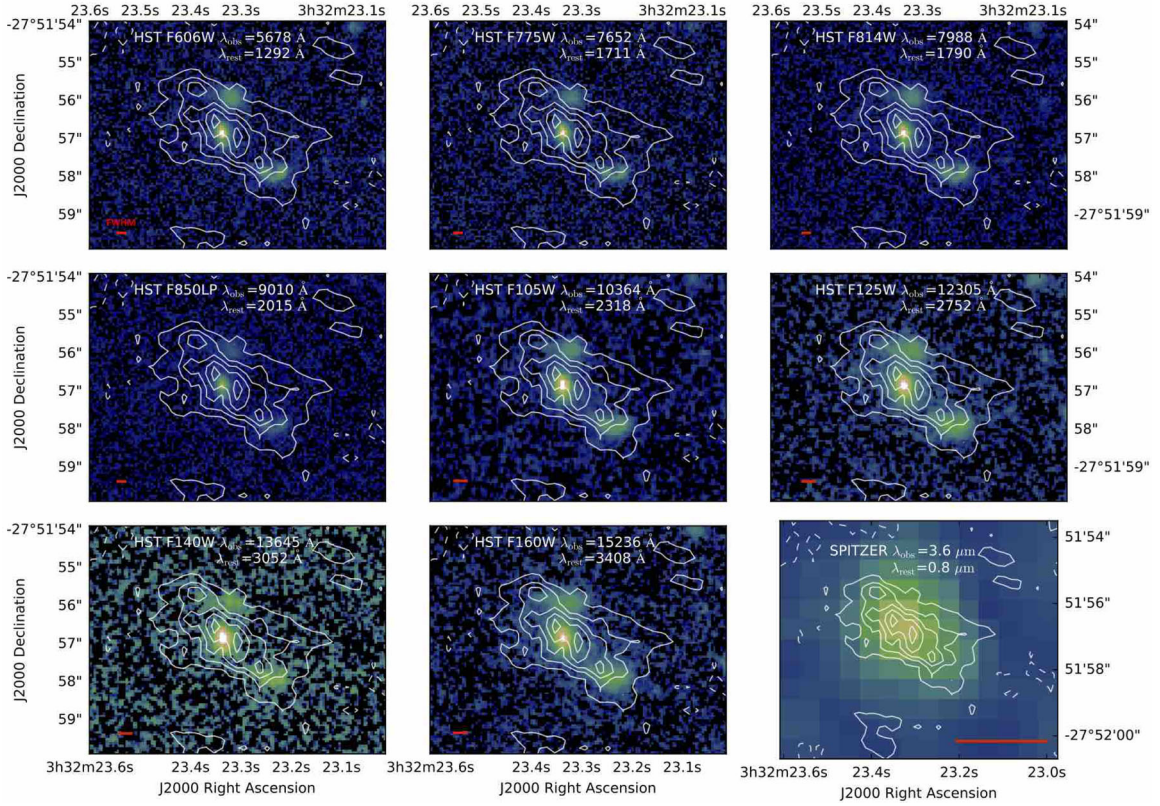
Figure B1. Overlay of CO emission with multiwavelength images of Candels-5001. The CO(4−3) emission is shown with contours (as in 3), while the colour background images show the available *HST* images (filter and rest-frame wavelength indicated within each panel) and the 3.6 μm *Spitzer* image (bottom-right). The red bar in each panel indicates the size of the *HST*/*Spitzer* PSF in that band.

this structure. The 3.6 μm *Spitzer* image (Fig. B1) has too low (2.5 arcsec) resolution to investigate the extended emission, which could not be disentangled from the contribution associated with the two satellite galaxies.

APPENDIX C: ANGULAR RESOLUTION EFFECTS CANDELS-5001

In Section 4.1, we claimed that the extended structure cannot be ascribed to molecular gas hosted in the three merging galaxies and 'artificially' smeared on a larger scale by the ALMA beam. We convolved the higher resolution [O III]5007 Å SINFONI map (Fig. 4) of Candels-5001 and its companions with the ALMA beam. In Fig. C1, we compare the spatial extension of the contours containing the 40 per cent and 80 per cent of the flux in the ALMA CO map with the same-level contours of the SIN-FONI smoothed images, confirming that beam smearing of putative molecular gas in the two satellite galaxies (along with the molecular gas in Candles-5001) cannot account for the observed CO extent.

## APPENDIX D: ADDITIONAL MAPS AND TABULATED PROPERTIES OF THE CO-EMITTING SYSTEMS

Figs D1 and D2 show the overlay of the CO emission observed in the systems detected on large scales with optical (*F775W*, *HST*),
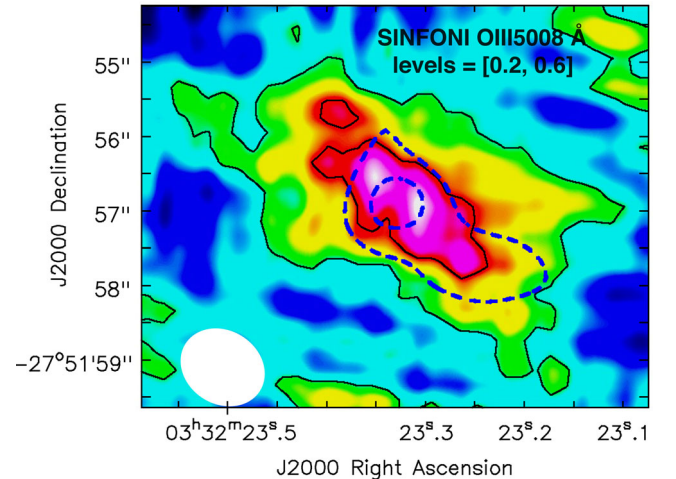

Figure C1. The background colour image is the CO map of the few tens kpc field around Candels-5001, obtained by ALMA. Black contours contain the 80 per cent and 40 per cent of the CO J = 4−3 flux. The blue dashed contours contain the 80 per cent and 40 per cent of the [O III] flux map obtained by smoothing the SINFONI/VLT data to the same resolution as the ALMA map.

near-IR (*F160W-HST* and 3.6 μm-*Spitzer*) and ALMA continuum images (see the text for discussion). Table D1 lists some basic properties of the CO systems on large scales, where line fluxes have been corrected for the primary beam response function.
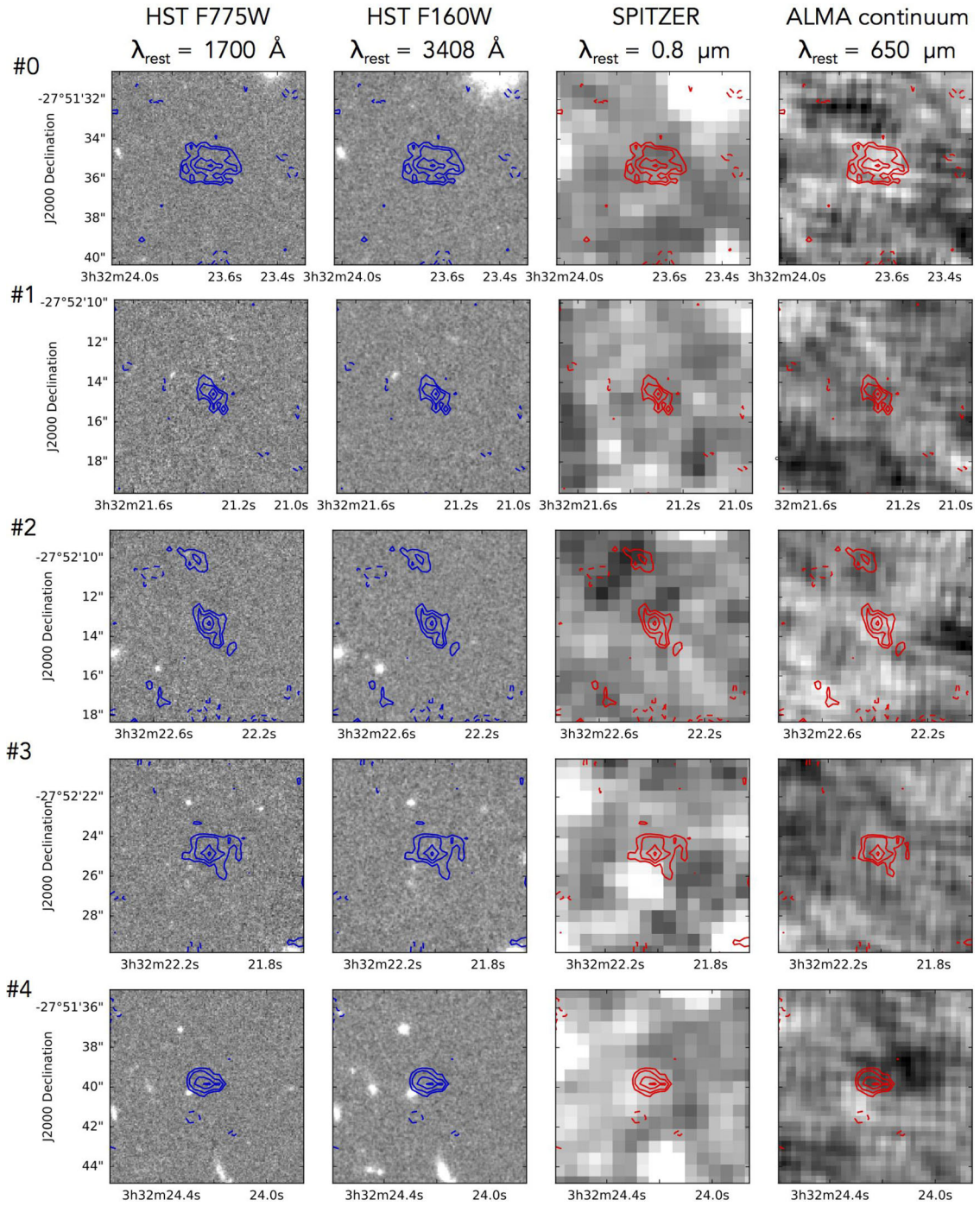
Figure D1. CO J = 4−3 maps (contours) of the individual systems detected on large scales overlaid on to the *HST*, *Spitzer* and ALMA continuum images. Objects no. 0–4.
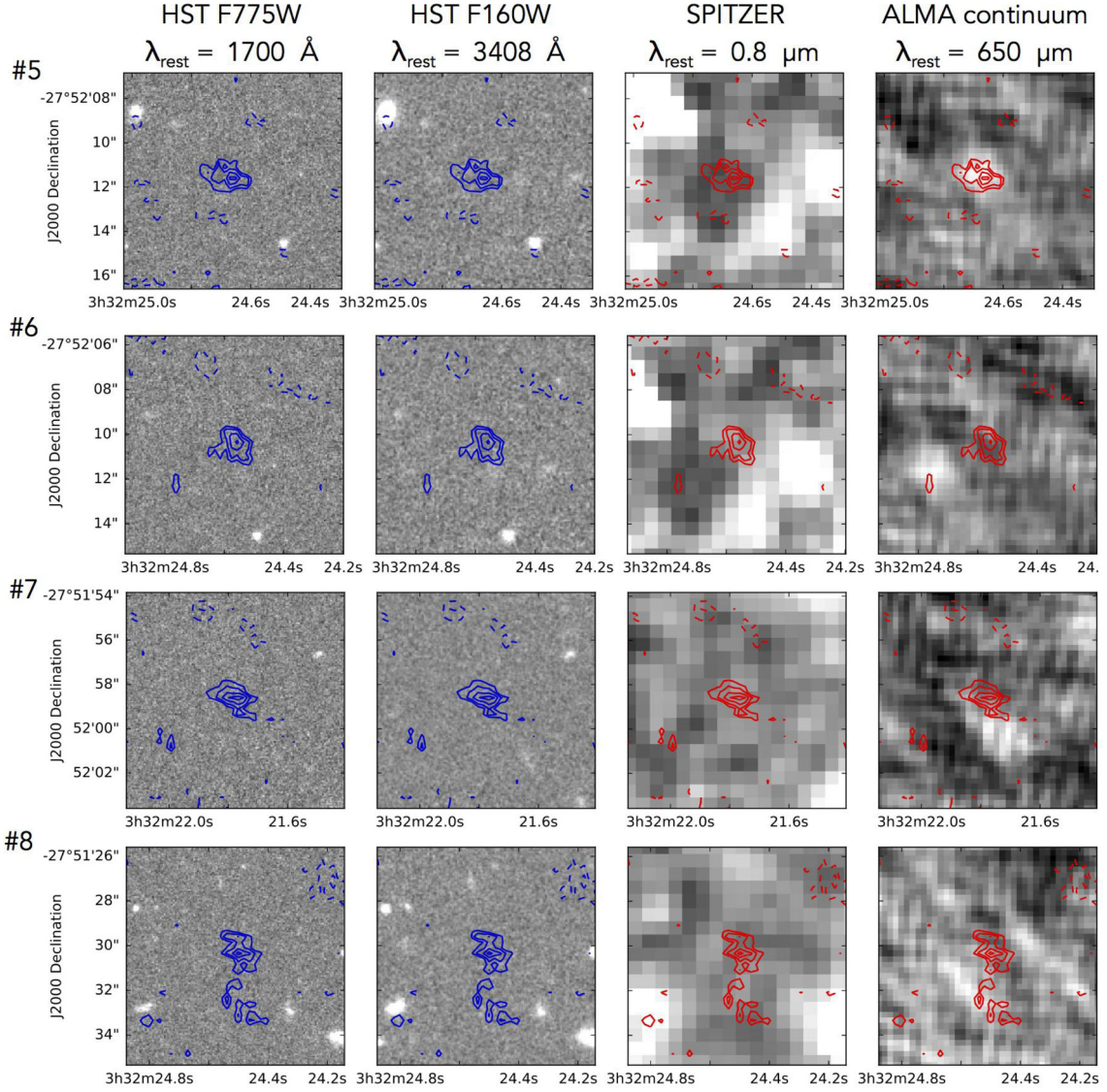
Figure D2. CO J = 4−3 maps (contours) of the individual systems detected on large scales overlaid on to the *HST*, *Spitzer* and ALMA continuum images. Objects no. 5–8.

Table D1. Summary of the properties of the CO systems detected on large scales.

ID	Right ascension J2000	Declination J2000	Line frequency CO J = 4−3 GHz	Line flux CO J = 4−3 Jy km s^{-1}	Line width CO J = 4−3 Jy km s^{-1}	Continuum flux μJy
no. 0	03:32:23.70	−27.51.33.8	102.72	0.110 ± 0.022	125	24.1 ± 9.6[a]
no. 1	03:32:21.34	−27.52.14.5	102.64	0.117 ± 0.022	100	<9.6
no. 2	03:32:22.44	−27.52.13.3	102.38	0.105 ± 0.012	131	22.3 ± 9.6[a]
no. 3	03:32:22.06	−27.52.24.8	103.10	0.202 ± 0.038	214	<9.6
no. 4	03:32:24.27	−27.51.39.8	103.05	0.104 ± 0.018	110	<9.6
no. 5	03:32:24.70	−27.52.11.5	102.85	0.107 ± 0.013	125	33.4 ± 9.6
no. 6	03:32:24.61	−27.52.10.3	103.85	0.102 ± 0.018	83	<9.6
no. 7	03:32:21.82	−27.51.58.5	103.75	0.136 ± 0.024	289	<9.6
no. 8	03:32:24.55	−27.51.30.3	103.83	0.116 ± 0.021	69	<9.6

[a]Marginal detections (∼2.5σ).

This paper has been typeset from a TEX/LATEX file prepared by the author.